nature research

https://doi.org/10.1038/s41551-020-00667-9

Supplementary information

Deep-learning-assisted analysis of echocardiographic videos improves predictions of all-cause mortality

In the format provided by the authors and unedited

Contents

List of Figures

List of Tables

1 Application to Stanford Dataset:

Ouyang et al. recently released a publicly available echocardiography video dataset with left ventricular ejection fraction (EF) measurements [34].Even though our models were trained for mortality prediction, we applied the AP4 model trained on the cross-validation set to the 10,030 publicly available videos to report the mortality risk as a function of EF.

To make the size and frame rate compatible with our trained models, we padded the original 112 pixels width with zeros to a size of 150 pixels and cropped the height from 112 to 109 pixels, and we resampled the frame rate to 30 frames per second with linear interpolation.

Using EF as a surrogate for mortality, we observed a trend similar to that reported in [40], see Supplementary Figure 10, where the risk of mortality is lowest at normal EF ranges, 50% to 65%, and increases for both lower and higher EF ranges.

For reproducibility purposes, we have published the code that conducts this experiment at the following code repository: `https://github.com/alvarouc/geisinger-echo-mortality`.

2 Comparison of cross-validation results with Samad et. al:

In our previous work [22], we conducted a cross-validation experiment for 1-year mortality prediction with a dataset of 331,317 echocardiography studies and reported an AUC of 0.85 AUC, 95% CI [0.84, 0.85] using tabular data only (compared to a reported AUC of 0.81 in our current paper for similar data inputs). To demonstrate that this performance difference between [22], and the current paper was driven by the sample size, we reproduced the cross-validation experiment 100 times by randomly sampling a subset of 42,095 echocardiography studies (equal to our cross-validation set size, see Supplementary Table 1) from the same set of 331,317 studies as in [22]. The average AUC across the 100 iterations was 0.812, 95% CI [0.810,0.814], which matches the reported performance in our limited dataset.

We had to limit our sample size in the current paper due to infrastructure capabilities. The DICOM file containing a single echocardiography study occupies approximately 1GB of disk space. Retrieving 331,317 studies would have demanded 331TB of disk storage. Currently, we do not have access to the required infrastructure to store and process this amount of echocardiography studies (in video form) as in [22].

3 Note on Echocardiography View Missingness:

In clinical practice, different specific views may be acquired during an echocardiogram as ordered by a cardiologist. The number of views obtained from the patient therefore may hold the potential to embed information on the patient likelihood of dying within a year. When deployed, a mortality risk model built from echocardiography video data should be robust to these potential video missingness patterns.

To enable support and robustness to missing videos, we incorporated an imputation step prior to the classification step, see Supplementary Figure 7. Thus, the classification step should not learn from missingness patterns. In order to confirm the robustness of the proposed model, we searched for evidence a relationship between the number of available videos and model performance. We grouped studies on each test set of the cross-validation folds into tertiles. Then, we tested the null hypothesis that at least one of the tertiles had a significantly different mean AUC. The tertile ranges were (0,19], (19,21], and (21,24], where the average

AUC for each group was 0.83, 0.86, and 0.85, respectively. Conducting an ANOVA test, we did not find evidence that at least one group had a significantly different mean ($p = 0.12$).

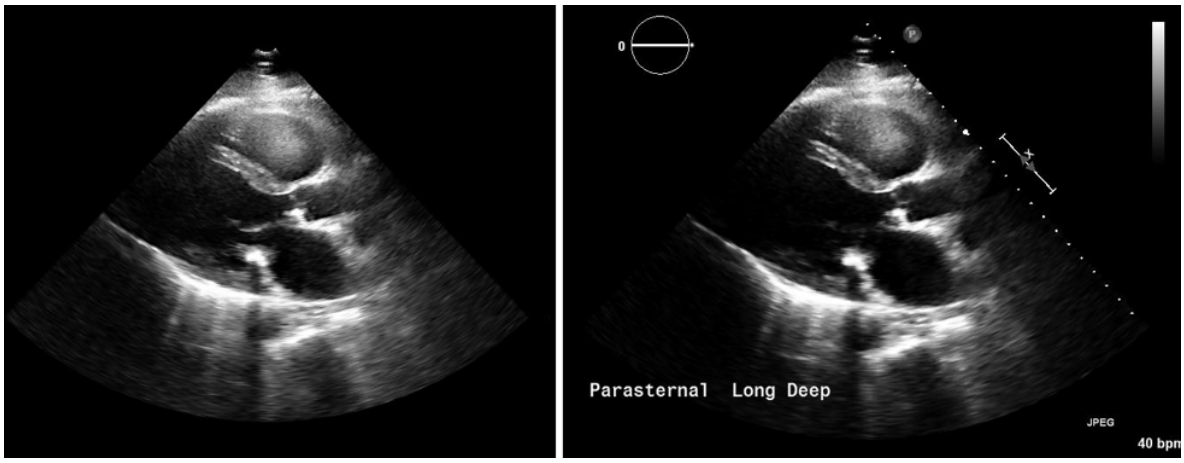

Supplementary Figure 1: Examples of raw (left) and annotated (right) videos.

Supplementary Figure 2: Interface of the web application developed for cardiologists to predict survival one year after echocardiography. Note that the annotated image shows a "87 bpm" marking that indicates the heart rate during the study while the extracted EHR data demonstrates a heart rate of 83 bpm as measured before the images were acquired.

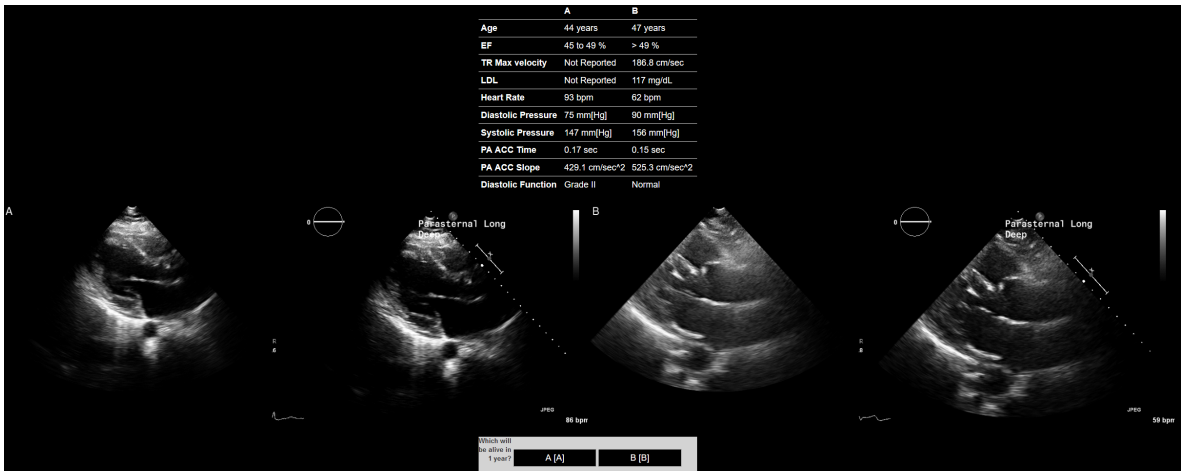

Supplementary Figure 3: Interface of the web application developed for cardiologists to predict survival one year after echocardiography on paired samples.

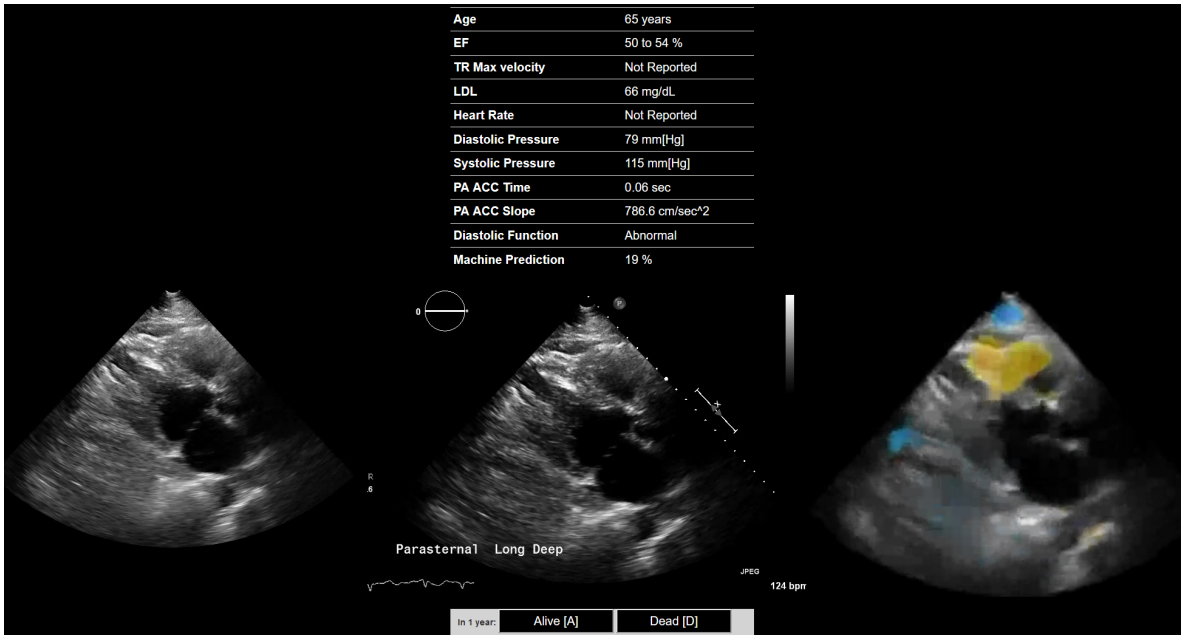

Supplementary Figure 4: Interface of the web application developed to assess the enhancement of cardiologists' prediction performance when provided with data from the DNN ("Machine Prediction" and the occlusion map findings (right panel).

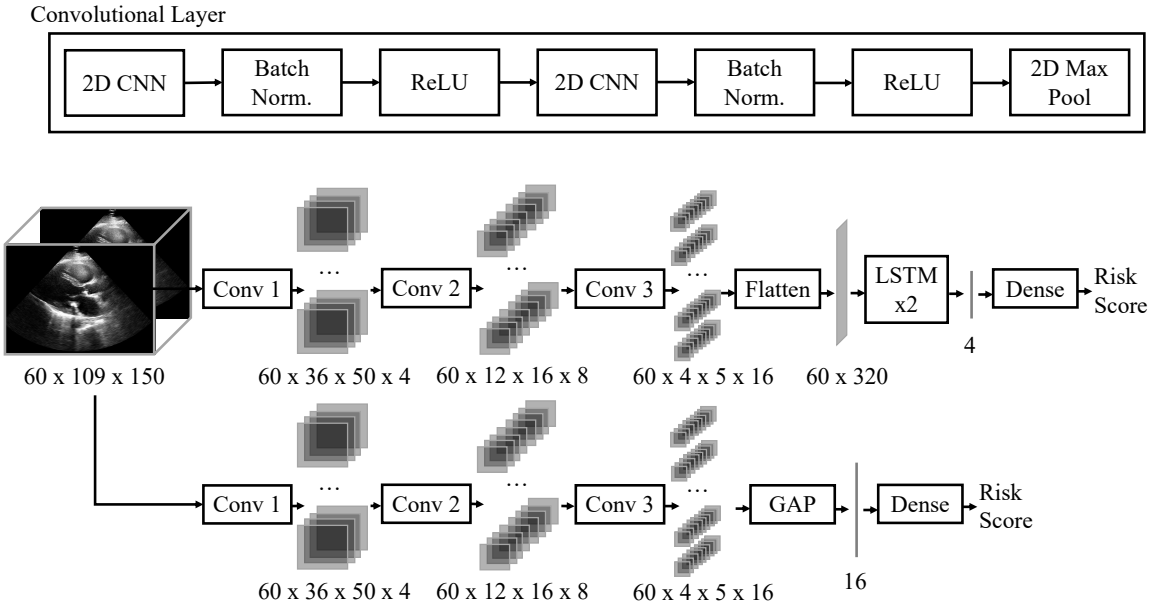

Supplementary Figure 5: 2D CNN-based Neural network architectures for mortality prediction from echocardiography videos. The convolutional layer (Conv) consists of Convolutional Neural Networks (CNN) with two-dimensional kernels, Batch Normalizations (Batch Norm.), rectified linear units (ReLU), and a two-dimensional Maximum Pooling layer (2D Max Pool). The Flatten layer takes the previous layer's activations and re-shapes them into a vector. The two Long short-term memory (LSTM) units shown take the 16 dimensional vector with 60 time steps and produces a static 4-dimensional vector, which is passed to a fully connected layer (Dense) with sigmoid activations and a Drop Out layer. The input video dimensions were 60 x 109 x 150 pixels, and the output dimensions of every layer are shown.

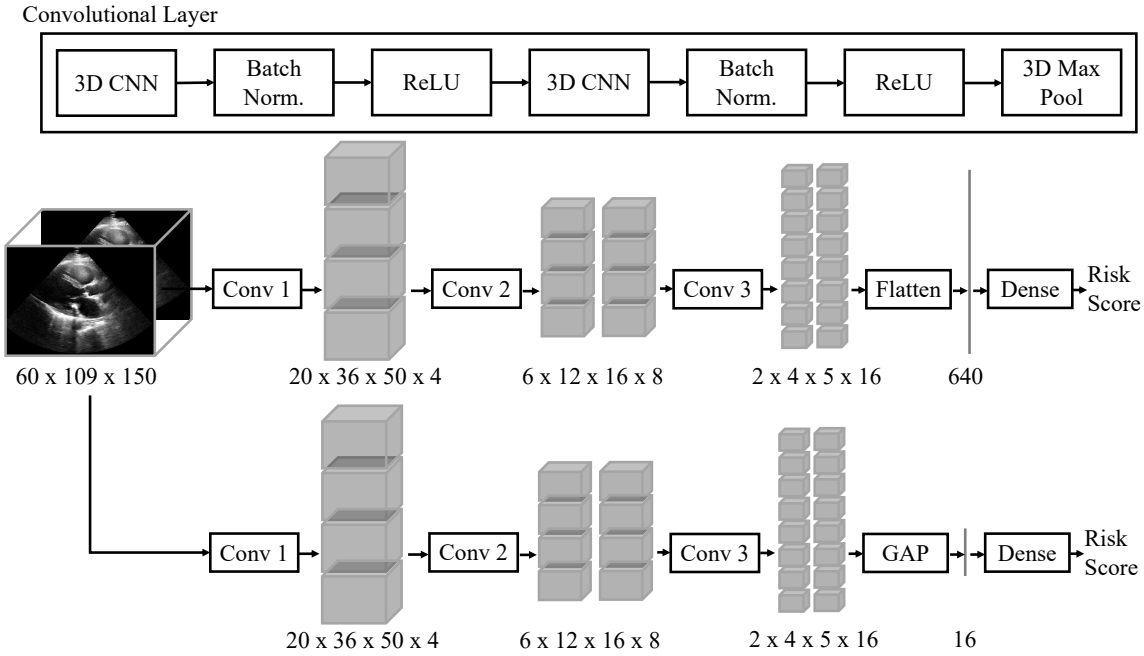

Supplementary Figure 6: 3D CNN-based Neural network architectures for mortality prediction from echocardiography videos. The convolutional layer (Conv) consists of Convolutional Neural Networks (CNN) with three-dimensional kernels, Batch Normalizations (Batch Norm.), rectified linear units (ReLU), and a three-dimensional Maximum Pooling layer (3D Max Pool). The Flatten layer takes the previous layer's activations and re-shapes them into a vector to pass to a fully connected layer (Dense) with sigmoid activations and a Drop Out layer. The input video dimensions were 60 x 109 x 150 pixels, and the output dimensions of every layer are shown.

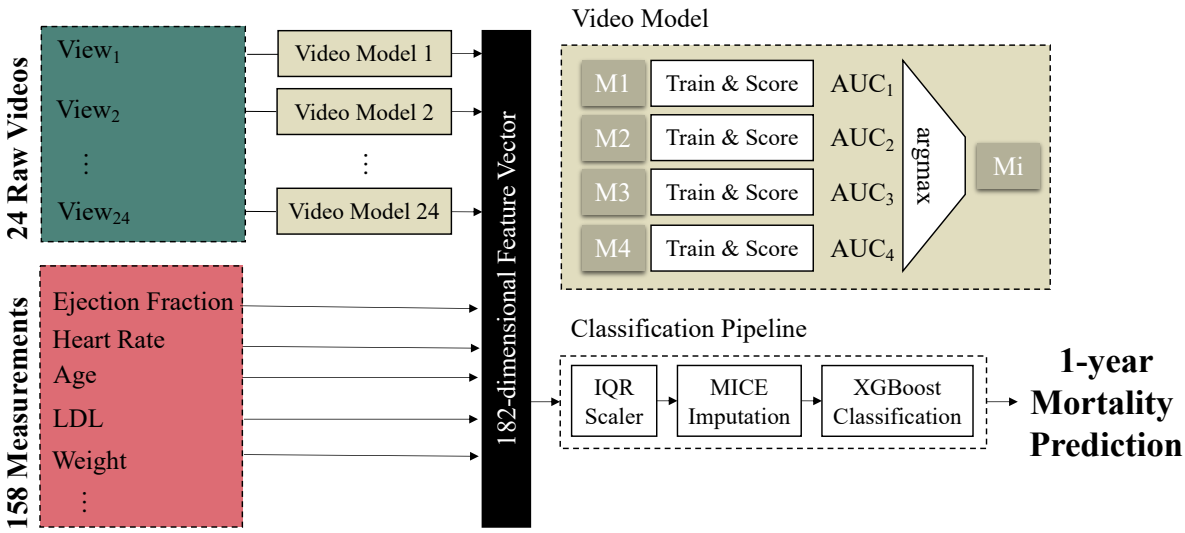

Supplementary Figure 7: Model diagram of the overall architecture that incorporates all echocardiography views and clinical variables, "All Views + EHR" model. The video model block describes the DNN model trained for a single echocardiography video view. For each view, the video model selects the best CNN architecture, M1-M4, by taking the architecture Mi that yielded the highest AUC in the validation set. The risk scores from each video model are concatenated to the EHR measurements to form the 182-dimensional feature vector, which is used to train the classification pipeline.

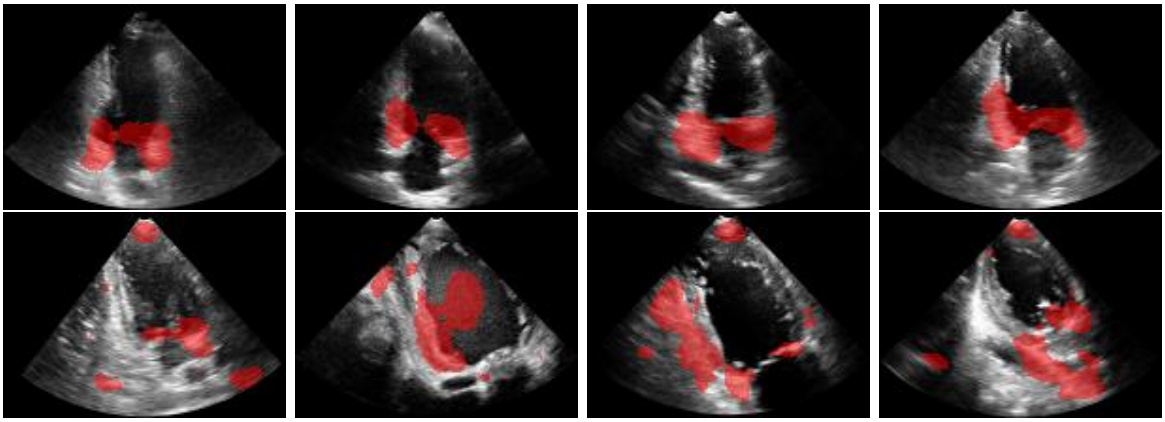

Supplementary Figure 8: Occlusion results for the four lowest (top) and four highest (bottom) prediction risk scores for one-year mortality obtained from an apical 2-chamber view. The red areas highlight regions that changed the risk score beyond 2.5 standard deviations (of all changes) for at least 10 frames. The red areas are overlayed on the first frame of the video for anatomical reference.

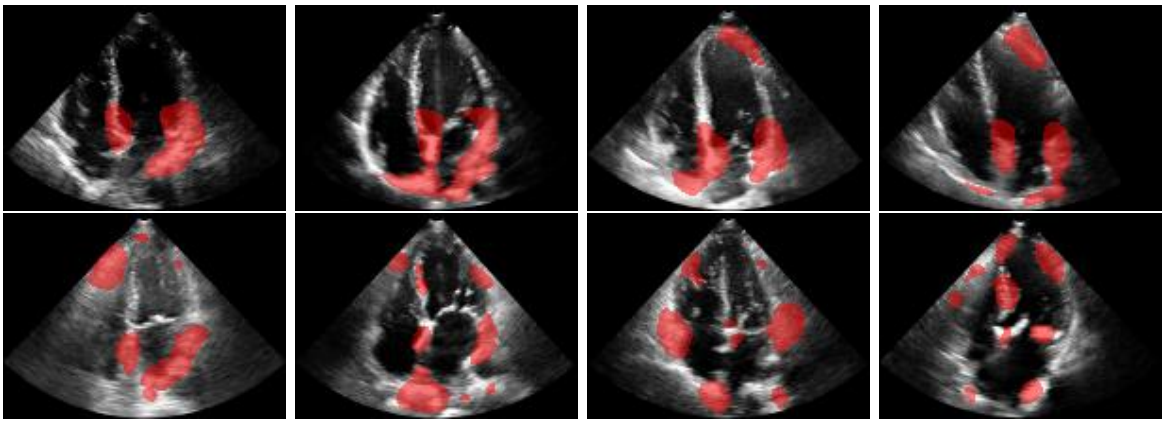

Supplementary Figure 9: Occlusion results for the four lowest (top) and four highest (bottom) prediction risk scores for one-year mortality obtained from an apical 4-chamber view. The red areas highlight regions that changed the risk score beyond 2.5 standard deviations (of all changes) for at least 10 frames. The red areas are overlayed on the first frame of the video for anatomical reference.

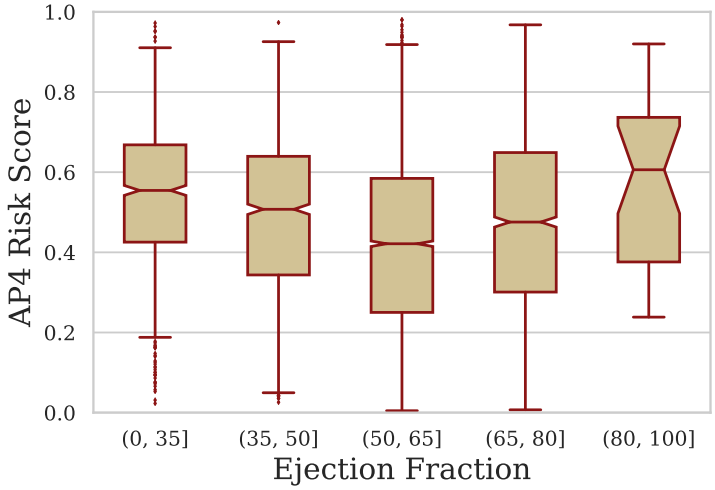

Supplementary Figure 10: Risk score produced by the apical four chamber (AP4) model trained on the cross-validation set vs (a) left ventricular ejection fraction, (b) end systolic volume, and (c) end diastolic volume for the 10,030 echocardiography videos published in [34], (N=10,030). The boxes denote the inter-quartile range (IQR) and whiskers extend quartiles by an IQR.

Supplementary Table 1: Summary statistics on the three groups of patients for all studies and for studies where the patient survived or died within a year of the study. We show the echocardiography study counts; percentage of males; average and standard deviation (in parenthesis) age, left ventricular ejection fraction, and body mass index; and percentage of studies where the patients presented with a diagnosis of heart failure, hypertension, or type II diabetes mellitus.

	Cross-validation			**Survey**			**Heart Failure**		
	All	Alive	Deceased	All	Alive	Deceased	All	Alive	Deceased
Count	42,095	35,963	6,132	600	300	300	3,384	2,435	949
Demographics									
Male	51.3%	50.6%	55.5%	55.5%	53.3%	57.7%	55.7%	56.3%	54.2%
Age	65.7(16.4)	64.4(16.4)	73.5(13.8)	68.4(16.2)	63.2(17.2)	73.7(13.2)	73.4(12.9)	71.8(13.0)	77.6(11.4)
LV Ejection Frac.	54.7(11.3)	55.4(10.4)	50.9(15.0)	53.5(12.8)	55.3(10.5)	51.7(14.5)	45.2(15.6)	46.0(15.1)	43.2(16.7)
BMI	30.8(8.0)	31.1(7.9)	29.1(8.3)	30.0(8.2)	31.3(8.5)	28.7(7.6)	31.6(8.4)	32.3(8.4)	29.8(8.2)
Co-morbidities									
Heart Failure	13.5%	10.4%	31.3%	21.5%	11.3%	31.7%	100%	100%	100%
Hypertension	72.7%	73.4%	68.3%	70.0%	73.7%	66.3%	85.8%	87.3%	82.0%
Type II Diabetes	29.6%	28.8%	33.8%	31.7%	29.3%	34.0%	47.3%	47.1%	47.7%

Supplementary Table 2: Low-parameter 2D CNN + LSTM with 15,409 trainable parameters and 112 non-trainable parameters from Batch Normalization (BN) layers

Layer	**# Parameters**	**Output Shape**	**Description**
		Convolutional Layer 1	
Conv 1.1	40	[60, 109, 150, 4]	4 2D feature maps
BN+ReLU	16	[60, 109, 150, 4]	Normalize feature maps
Conv 1.2	148	[60, 109, 150, 4]	4 2D feature maps
BN+ReLU	16	[60, 109, 150, 4]	Normalize feature maps
Max Pool	-	[60, 36, 50, 4]	3x3 max-pooling
		Convolutional Layer 2	
Conv 2.1	296	[60, 36, 50, 8]	8 2D feature maps
BN+ReLU	32	[60, 36, 50, 8]	Normalize feature maps
Conv 2.2	584	[60, 36, 50, 8]	8 2D feature maps
BN+ReLU	32	[60, 36, 50, 8]	Normalize feature maps
Max Pool	-	[60, 12, 16, 8]	3x3 max-pooling
		Convolutional Layer 3	
Conv 3.1	1,168	[60, 12, 16, 16]	16 2D feature maps
BN+ReLU	64	[60, 12, 16, 16]	Normalize feature maps
Conv 3.2	2,320	[60, 12, 16, 16]	16 2D feature maps
BN+ReLU	64	[60, 12, 16, 16]	Normalize feature maps
Max Pool	-	[60, 4, 5, 16]	3x3 max-pooling
		LSTM Layers	
Flatten	-	[60, 320]	Reshape to vectors
LSTM 1	10,528	[60, 8]	60 step LSTM
LSTM 2	208	[4]	Last state LSTM
		Output Layer	
Dropout	-	[4]	50% Dropout
Dense+Sigmoid	5	[1]	Logit to Output

Supplementary Table 3: Low-parameter 2D CNN + GAP with 4,685 trainable parameters and 112 non-trainable parameters from Batch Normalization (BN) layers.

Layer	**# Parameters**	**Output Shape**	**Description**
		Convolutional Layer 1	
Conv 1.1	40	[60, 109, 150, 4]	4 2D feature maps
BN+ReLU	16	[60, 109, 150, 4]	Normalize feature maps
Conv 1.2	148	[60, 109, 150, 4]	4 2D feature maps
BN+ReLU	16	[60, 109, 150, 4]	Normalize feature maps
Max Pool	-	[60, 36, 50, 4]	3x3 max-pooling
		Convolutional Layer 2	
Conv 2.1	296	[60, 36, 50, 8]	8 2D feature maps
BN+ReLU	32	[60, 36, 50, 8]	Normalize feature maps
Conv 2.2	584	[60, 36, 50, 8]	8 2D feature maps
BN+ReLU	32	[60, 36, 50, 8]	Normalize feature maps
Max Pool	-	[60, 12, 16, 8]	3x3 max-pooling
		Convolutional Layer 3	
Conv 3.1	1,168	[60, 12, 16, 16]	16 2D feature maps
BN+ReLU	64	[60, 12, 16, 16]	Normalize feature maps
Conv 3.2	2,320	[60, 12, 16, 16]	16 2D feature maps
BN+ReLU	64	[60, 12, 16, 16]	Normalize feature maps
Max Pool	-	[60, 4, 5, 16]	3x3 max-pooling
		Output Layer	
GAP	-	[16]	Global average Pooling
Dropout	-	[16]	50% Dropout
Dense+Sigmoid	17	[1]	Logit to Output

Supplementary Table 4: Low-parameter Dyadic 3D CNN with 14,309 trainable and 112 non-trainable parameters from Batch Normalization (BN) layers.

Layer	**# Parameters**	**Output Shape**	**Description**
		Convolutional Layer 1	
Conv 1.1	112	[60, 109, 150, 4]	4 3D feature maps
BN+ReLU	16	[60, 109, 150, 4]	Normalize feature maps
Conv 1.2	436	[60, 109, 150, 4]	4 3D feature maps
BN+ReLU	16	[60, 109, 150, 4]	Normalize feature maps
Max Pool	-	[20, 36, 50, 4]	3x3x3 max-pooling
		Convolutional Layer 2	
Conv 2.1	872	[20, 36, 50, 8]	8 3D feature maps
BN+ReLU	32	[20, 36, 50, 8]	Normalize feature maps
Conv 2.2	1,736	[20, 36, 50, 8]	8 3D feature maps
BN+ReLU	32	[20, 36, 50, 8]	Normalize feature maps
Max Pool	-	[6, 12, 16, 8]	3x3 max-pooling
		Convolutional Layer 3	
Conv 3.1	3,472	[6, 12, 16, 16]	16 3D feature maps
BN+ReLU	64	[6, 12, 16, 16]	Normalize feature maps
Conv 3.2	6,928	[6, 12, 16, 16]	16 3D feature maps
BN+ReLU	64	[6, 12, 16, 16]	Normalize feature maps
Max Pool	-	[2, 4, 5, 16]	3x3 max-pooling
		Output Layer	
Flatten	-	[640]	Reshape to vector
Dropout	-	[640]	50% Dropout
Dense+Sigmoid	641	[1]	Logit to Output

Supplementary Table 5: Low-parameter Dyadic 3D CNN + GAP with 13,685 trainable and 112 non-trainable parameters from Batch Normalization (BN) layers.

Layer	**# Parameters**	**Output Shape**	**Description**
Convolutional Layer 1			
Conv 1.1	112	[60, 109, 150, 4]	4 3D feature maps
BN+ReLU	16	[60, 109, 150, 4]	Normalize feature maps
Conv 1.2	436	[60, 109, 150, 4]	4 3D feature maps
BN+ReLU	16	[60, 109, 150, 4]	Normalize feature maps
Max Pool	-	[20, 36, 50, 4]	3x3x3 max-pooling
Convolutional Layer 2			
Conv 2.1	872	[20, 36, 50, 8]	8 3D feature maps
BN+ReLU	32	[20, 36, 50, 8]	Normalize feature maps
Conv 2.2	1,736	[20, 36, 50, 8]	8 3D feature maps
BN+ReLU	32	[20, 36, 50, 8]	Normalize feature maps
Max Pool	-	[6, 12, 16, 8]	3x3 max-pooling
Convolutional Layer 3			
Conv 3.1	3,472	[6, 12, 16, 16]	16 3D feature maps
BN+ReLU	64	[6, 12, 16, 16]	Normalize feature maps
Conv 3.2	6,928	[6, 12, 16, 16]	16 3D feature maps
BN+ReLU	64	[6, 12, 16, 16]	Normalize feature maps
Max Pool	-	[2, 4, 5, 16]	3x3 max-pooling
Output Layer			
GAP	-	[16]	Global average Pooling
Dropout	-	[16]	50% Dropout
Dense+Sigmoid	17	[1]	Logit to Output

Supplementary Table 6: View labels found in DICOM headers for the corresponding view type.

CODE	VIEW TYPE	**VIEW LABELS**
A2	Apical 2	a2, ap2 2d, a2 2d, a2 lavol, la 2ch
A LONG	Apical 3	a long, ap3 2d, a3 2d
AP4	Apical 4	ap4, ap4 2d, a4 2d, a4 zoom, a4 lavol, la ap4 ch
RV FOCUS	Apical 4 focused to rv	rv focus, rvfocus
A5	Apical 5	a5, ap5 2d, a5 2d
PL DEEP	Parasternal long axis	pl deep, psl deep
PL ASCAO	Parasternal long ascending aorta	pl ascao, asc ao, pl asc ao
PLA MV	Parasternal long mitral valve	pla mv
PL PV	Parasternal long pulmonic valve	pl pv, pv lax
PL RVIF	Parasternal long rv inflow	pl rvif, rv inf, rvif 2d
PL AV AO	Parasternal long zoom aortic valve	pl av ao, av zoom
PS AV	Parasternal short aortic valve	ps av, psavzoom, psax av
PS PV PA	Parasternal short pulmonic valve and pulmonary artery	ps pv pa, ps pv, psax pv
PS TV	Parasternal short tricuspid valve	ps tv, ps tv 2d, psax tv
SAX APEX	Short axis apex	sax apex
LV BASE	Short axis base	lv base
SAX MID*	Short axis mid papillary	sax mid, sax
SBC 4 CH	Subcostal 4 chamber	sbc 4 ch, sbc 4, sbc 4ch
IVC HV	Subcostal hepatic vein	ivc hv, sbc hv
IAS	Subcostal inter-atrial septum	ias, sbc ias, ias 2d
IVC RESP	Subcostal ivc with respiration	ivc resp, sbc ivc, ivc insp,ivc snif, ivcsniff, sniff
SBC RV	Subcostal rv	sbc rv
SSN*	Suprasternal notch	ssn, ssn sax
LV MID	Short axis mid papillary	lv mid
LV APEX	Short axis apex	lv apex
SAX BASE*	Short axis base	sax base

* Views excluded from analysis due to lack of samples to train.

Supplementary Table 7: Table notation for the 8 models derived from the 4 core architectures reported in Supplementary Tables 2, 3, 4, and 5.

	Kernel size	
Name	3x3x3	5x5x5
3D CNN	3D	$3D_5$
3D CNN + GAP	$3D^{GAP}$	$3D_5^{GAP}$
2D CNN + LSTM	$2D^{LSTM}$	$2D_5^{LSTM}$
2D CNN + GAP	$2D^{GAP}$	$2D_5^{GAP}$

Supplementary Table 8: Selected neural network arhitecture for each view and fold, including the final model that trains on all folds, in the cross-validation experiment. See view name abbreviation in Supplementary Table 6 and model naming notation in Supplementary Table 7. Among the 24 video models and 5 folds (120 trainings) the 3D architecture was chosen 56 times (34 and 22 for the kernel sizes 3 and 5), 3D+GAP was chosen 53 times (39 and 14), 2D+GAP was chosen 9 times and 2D+LSTM was chosen 2 times.

View	Fold 1	Fold 2	Fold 3	Fold 4	Fold 5	Final
A LONG	$3D^{GAP}$	3D	3D	$3D_5^{GAP}$	$3D^{GAP}$	$3D_5$
A2	3D	3D	$3D^{GAP}$	$3D_5^{GAP}$	$3D_5^{GAP}$	$3D_5$
A5	$3D_5$	$3D_5$	$3D^{GAP}$	$3D_5$	$3D_5$	$3D_5$
AP4	$3D_5^{GAP}$	$3D_5$	$3D_5$	3D	$3D_5^{GAP}$	$3D_5^{GAP}$
IAS	$3D_5$	$3D^{GAP}$	3D	$3D_5^{GAP}$	$3D^{GAP}$	$3D_5$
IVC HV	$2D^{GAP}$	$3D^{GAP}$	3D	3D	$2D^{GAP}$	$3D^{GAP}$
IVC RESP	$3D^{GAP}$	$2D^{GAP}$	$2D^{GAP}$	3D	$3D_5$	$3D^{GAP}$
LV APEX	$3D^{GAP}$	$3D^{GAP}$	$3D_5^{GAP}$	3D	$3D_5$	$3D^{GAP}$
LV BASE	3D	$3D^{GAP}$	$3D^{GAP}$	3D	3D	$3D_5$
LV MID	$3D^{GAP}$	$3D_5$	$3D_5$	$3D^{GAP}$	3D	$3D_5^{GAP}$
PL ASCAO	$3D_5^{GAP}$	$3D^{GAP}$	$3D_5^{GAP}$	$3D^{GAP}$	$3D^{GAP}$	3D
PL AV AO	$3D_5$	$3D^{GAP}$	3D	$3D^{GAP}$	$3D^{GAP}$	$3D_5$
PL DEEP	3D	$3D_5$	3D	$3D_5^{GAP}$	$3D^{GAP}$	3D
PL PV	$2D^{GAP}$	3D	3D	3D	3D	$3D_5$
PL RVIF	$3D^{GAP}$	$3D_5^{GAP}$	3D	$3D^{GAP}$	$3D_5$	3D
PL ZOOM	$3D_5$	$3D^{GAP}$	$3D_5$	$3D_5$	$3D_5$	$3D_5$
PLA MV	$3D_5^{GAP}$	$3D^{GAP}$	$3D_5^{GAP}$	$2D^{LSTM}$	$2D^{GAP}$	3D
PS AV	3D	3D	$3D_5^{GAP}$	3D	$3D^{GAP}$	$3D_5$
PS PV PA	3D	3D	$3D_5$	3D	$3D^{GAP}$	$3D^{GAP}$
PS TV	$3D^{GAP}$	$3D^{GAP}$	$3D_5$	$3D^{GAP}$	$3D_5$	3D
RV FOCUS	$3D_5$	3D	$3D^{GAP}$	3D	$3D^{GAP}$	$3D_5$
SBC 4 CH	$3D^{GAP}$	$3D^{GAP}$	3D	3D	$3D^{GAP}$	3D
SBC RV	$3D^{GAP}$	3D	$3D^{GAP}$	$3D^{GAP}$	$3D^{GAP}$	3D
SSN	$2D^{GAP}$	$2D^{LSTM}$	3D	$2D^{GAP}$	$2D^{GAP}$	$3D_5$

Supplementary Table 9: AUC in percentage for the PL DEEP view on each fold, cross-validation set, and architecture. At each fold, the architecture with the best validation AUC (in bold font) is used to report the test AUC.

Fold	Set	$2D^{GAP}$	$2D^{LSTM}$	$3D^{GAP}$	3D	$3D_5$	$3D_5^{GAP}$
1	Train	80.6	83.1	83.2	82.1	86.0	83.3
	Validation	78.1	77.1	80.0	**80.1**	79.9	78.6
	Test	77.5	77.1	79.1	79.7	79.2	78.5
2	Train	82.7	82.8	82.2	81.5	84.4	83.1
	Validation	77.4	76.8	78.4	78.9	**79.2**	78.0
	Test	78.0	77.7	79.8	79.9	79.9	79.4
3	Train	82.3	82.7	83.7	84.5	84.2	81.2
	Validation	77.0	75.5	78.8	**79.2**	78.5	76.7
	Test	78.0	76.5	79.4	79.6	78.4	77.4
4	Train	82.9	84.1	82.7	84.3	82.9	82.7
	Validation	78.2	77.4	80.1	79.4	79.5	**80.1**
	Test	76.8	75.3	79.4	78.1	78.0	78.7
5	Train	82.0	80.8	83.8	84.1	85.1	83.7
	Validation	76.5	75.8	**79.1**	78.0	77.8	77.2
	Test	77.5	76.7	78.6	78.8	78.4	77.8
Final	Train	81.4	82.3	83.2	84.0	84.4	82.3
	Validation	79.2	78.7	80.6	**80.8**	80.3	79.5

Supplementary Table 10: Distribution of number of echocardiography studies per patient in the cross-validation set.

# Studies	# Patients
1	28611
2	4344
3	1013
4	269
5	86
6	25
7	12
9	1
8	1

Supplementary Table 11: Distribution of number of videos per echocardiography study in the cross-validation set grouped by tertiles.

Tertile	# Views	# Studies	Total
I	1	445	15,892
	2	376	
	3	110	
	4	88	
	5	159	
	6	212	
	7	68	
	8	102	
	9	174	
	10	359	
	11	607	
	12	240	
	13	235	
	14	293	
	15	493	
	16	886	
	17	1,596	
	18	2,947	
	19	6,502	
II	20	8,879	13,187
	21	4,308	
III	22	8,790	13,016
	23	2,973	
	24	1,253	

Supplementary Table 12: Description of all variables extracted from the electronic health records, including structured echocardiography measurements. *MOD = modified ellipsoid, **el = (single plane) ellipsoid, LV = left ventricular, IV = inter-ventricular. Superscripts [1–10] denote selected EHR variables previously reported as the top 10 predictors of 1-year mortality [22]. *Hot encoded for severity levels 0,1,2,3 and -1 for not assessed. Diastolic function coding -1: Normal, 0: abnormal (no grade reported), [1,2,3]: grade I/II/III

	EHR VARIABLE	UNITS	DESCRIPTION
	Demographics		
1	Age[1]	years	At the time of study
2	Sex	0/1	0: Female, 1: Male
3	Smoking status	0/1	0: Never smoked
	Vitals		
4	Height	cm	
5	Weight	kg	
6	Heart rate[3]	bpm	
7	Diastolic blood pressure[6]	mm Hg	
8	Systolic blood pressure[8]	mm Hg	
	Laboratory		
9	LDL[4]	mg/DL	Low-density lipoprotein
10	HDL	mg/DL	High-density lipoprotein
	Echocardiography measurements		
11	LVEF[5]	%	Physician-reported left ventricular ejection fraction
12	AI dec slope	cm/s^2	Aortic insufficiency deceleration slope
13	AI max vel	cm/s	Aortic insufficiency max. velocity
14	Ao V2 VTI	cm	Velocity-time integral of distal to aortic valve flow
15	Ao V2 max	cm/s	Max. velocity of distal to aortic valve flow
16	Ao V2 mean	cm/s	Mean velocity of distal to aortic valve flow
17	Ao root diam	cm	Aortic root diameter
18	Asc Aorta	cm	Ascending aortic diameter
19	EDV MOD*- sp2	ml	LV end-diastolic vol.: apical 2-chamber
20	EDV MOD*- sp4	ml	LV end-diastolic vol.: apical 4-chamber
21	EDV sp2-el**	ml	LV end-diastolic vol.: apical 2-chamber
22	EDV sp4-el**	ml	LV end-diastolic vol.: apical 4-chamber
23	ESV MOD*-sp2	ml	LV end-systolic vol.: apical 2-chamber
24	ESV MOD*-sp4	ml	LV end-systolic vol.: apical 4-chamber
25	ESV sp2-el**	ml	LV end-systolic vol.: apical 2-chamber
26	ESV sp4-el**	ml	LV end-systolic vol.: apical 4-chamber
27	IVSd	cm	IV septum dimension at end-diastole

28	LA dimension	cm	Left atrium dimension
29	LAV MOD*-sp2	ml	Left atrium volume: apical 2-chamber
30	LAV MOD*-sp4	ml	Left atrium volume: apical 4-chamber
31	LV V1 VTI	cm	Velocity-time integral: proximal to the obstruction
32	LV V1 max	cm/s	Max. LV velocity: proximal to the obstruction
33	LV V1 mean	cm/s	Mean LV velocity proximal to the obstruction
34	LVAd ap2	cm^2	LV area at end-diastole: apical 2-chamber
35	LVAd ap4	cm^2	LV area at end-diastole: apical 4-chamber
36	LVAs ap2	cm^2	LV area at end-systole: apical 2-chamber
37	LVAs ap4	cm^2	LV area at end-systole: apical 4-chamber
38	LVIDd	cm	LV internal dimension at end-diastole
39	LVIDs	cm	LV internal dimension at end-systole
40	LVLd ap2	cm	LV long-axis length at end-diastole: apical 2-chamber
41	LVLd ap4	cm	LV long-axis length at end-diastole: apical 4-chamber
42	LVLs ap2	cm	LV long-axis length at end systole: apical 2-chamber
43	LVLs ap4	cm	LV long-axis length at end systole: apical 4-chamber
44	LVOT area M	cm^2	LV outflow tract area
45	LVOT diam	cm	LV outflow tract diameter
46	LVPWd	cm	LV posterior wall thickness at end-diastole
47	MR max vel	cm/s	Mitral regurgitation max. velocity
48	MV A point	cm/s	A-point max. velocity of mitral flow
49	MV E point	cm/s	E-point max. velocity of mitral flow
50	MV P1/2t max-vel	cm/s	Max. velocity of mitral valve flow
51	MV dec slope	cm/s^2	Mitral valve deceleration slope
52	MV dec time	s	Mitral valve deceleration time
53	PA V2 max	cm/s	Max. velocity of distal to pulmonic valve flow
54	PA acc slope9	cm/s^2	Pulmonary artery acceleration slope
55	PA acc time7	s	Pulmonary artery acceleration time
56	Pulm. R-R	s	Pulmonary R-R time interval
57	RAP systole	mm-Hg	Right atrial end-systolic mean pressure
58	RVDd	cm	Right ventricle dimension at end-diastole
59	TR max vel^2	cm/s	Tricuspid regurgitation max. velocity
60	AVR	0/1*	Aortic valve regurgitation
61	MVR	0/1*	Mitral valve regurgitation
62	TVR	0/1*	Tricuspid valve regurgitation
63	PVR	0/1*	Pulmonary valve regurgitation
64	AVS	0/1*	Aortic valve stenosis
65	MVS	0/1*	Mitral valve stenosis
66	TVS	0/1*	Tricuspid valve stenosis
67	PVS	0/1*	Pulmonary valve stenosis

68	Diastolic function[10]	-1, 0, 1, 2, 3, 4	Physician-reported diastolic function
	Diagnosis codes		
69-71	I00, I01, I02		Acute rheumatic fever
72-76	I05, I06, I07, I08, I09		Chronic rheumatic heart disease
77-82	I10, I11, I12, I13, I15, I16		Hypertensive diseases
83-88	I20, I21, I22, I23, I24, I25		Ischemic heart diseases
89-91	I26, I27, I28		Pulmonary heart disease and diseases of pulmonary circulation
92	I30		Acute pericarditis
93-106	I31, I32, I33, I34, I35, I36, I37, I38, I39, I43, I44, I45, I49, I51		Other forms of heart disease
107	I40		Acute myocarditis
108	I42		Cardiomyopathy
109	I46		Cardiac arrest
110	I47		Paroxysmal tachycardia
111	I48		Atrial fibrillation
112	I50		Heart failure
113-121	I60, I61, I62, I63, I65, I66, I67, I68, I69		Cerebrovascular diseases
122-131	I70, I71, I72, I73, I74, I75, I76, I77, I78, I79		Diseases of arteries, arterioles and capillaries
131-140	I80, I81, I82, I83, I85, I86, I87, I88, I89		Diseases of veins, lymphatic vessels, and lymph nodes
141	I95		Hypotension
142-144	I96, I97, I99		Other and unspecified disorders of the circulatory system
145-149	E08, E09, E10, E11, E13		Diabetes mellitus
150-156	Q20, Q21, Q22, Q23, Q24, Q25, Q26		Congenital heart defect
157	E78		Dyslipidemia
158	N18		Chronic kidney disease